Pose-Following with Dual Quaternions

Jon Arrizabalaga[1] and Markus Ryll[1,2]

***Abstract*— The focus of this work is on pose-following, a variation of path-following that involves guiding the system's position and orientation along a path with a moving frame attached to it. Achieving full-body motion control while simultaneously allowing for self-regulation of the path's progress represents an attractive trade-off. To this end, we have extended the well-established dual quaternion-based pose-tracking method to a pose-following control law. Specifically, we derive the equations of motion for the complete pose error between the geometric reference and the rigid body in the form of dual quaternion and dual twist, and subsequently develop an almost globally asymptotically stable pose-following control law. The resulting stability properties are validated by conducting simulations in an spatial illustrative case-study across a wide range of initial conditions, while its benefits over pose-tracking are showcased through a planar comparison.**

I. INTRODUCTION

Concurrent attitude and position – *pose* – control of a rigid body in three-dimensional space is crucial to many applications, such as for autonomous vehicles or robotic manipulators.

The straightforward approach to address the pose control problem is dividing it into two separate subproblems [1]–[3]. On the one hand, a *position controller* drives the translational motions, and on the other hand, an *attitude controller* regulates the rotational behavior. This decoupling relates to the standard representation of the rigid body dynamics, in which the translational and angular motions are expressed separately (as planar and spatial examples, see eq. 7 in [4] and eq. 1 in [5]). However, such partitioning poses a challenge to effectively control the interdependence between the rotational and translational dynamics.

Another option is representing the system dynamics globally on the configuration manifold of the special Euclidean group $\mathrm{SE}(3)$. Doing so allows for leveraging the group structure to first avoid singularities and second extend proportional derivative (PD) feedback controllers, for the pose-tracking problem [6]. Control methods inspired by these findings have shown very promising results within a plethora of robotic platforms, such as quadrotors [7]–[9], robotic manipulators [10], [11], walking robots [12] and spacecrafts [13], [14].

When describing a rigid body in $\mathrm{SE}(3)$, it is common to combine a three-dimensional vector of the Cartesian coordinates with either a rotation matrix – resulting in a homogeneous transformation matrix (HTM) – or a unit quaternion. A less common choice are *unit dual quaternions*, which have been applied across a wide range of disciplines, including but not limited to inertial navigation [15], state estimation [16], inverse kinematics [17], computer graphics [18] and computer vision [19].

Regarding pose control, akin to [6], the authors in [20] and [21] broadened PD-alike feedback controllers to encompass the Lie group of unit dual using its logarithmic mapping. This resulted in a globally exponentially stable kinematic control law for pose regulation or tracking. These outcomes were subsequently expanded in [22] to also account for rigid body dynamics. Since these findings, the unit dual quaternion-based pose-tracking problem has received considerable attention in the literature [14], [23]–[29].

In spite of these achievements, all these methods exclusively focus on *pose-tracking*, i.e., they track a time-varying position and attitude reference. However, not all problems fit in such a description. Following the illustrative example from [30], when precisely steering a robot's tool along a geometric reference, the primary concern is to minimize the deviation between the reference and the tool, while the velocity to move along the reference is of secondary interest and can be modified to enhance accuracy. In other words, the problem is not centered on tracking a pre-defined time-varying reference, but rather on leveraging the velocity to traverse the reference as an additional degree of freedom. Such control problems are denoted as *path-following*. This allows for overcoming the fundamental limitations of reference-tracking [31] and accounts for the significant attention path-following has received in literature. A detailed description of existing approaches can be found in [30]. Among those, most of the existing path-following methods omit the rotational dynamics and focus on path convergence of the translational dynamics.

Aiming to close this gap, we assume that the geometric reference consists of a desired path with a moving coordinate frame associated to it, and we define *pose-following* as a generalization of path-following in which the goal is to drive the system's position and attitude along the reference. This raises the question of how to formulate such a pose-following method.

To answer this question, in this paper we derive a unit dual quaternion-based pose-following control approach for rigid body dynamics. To this end, we take advantage of the benefits of unit dual quaternions, namely singularity-free, compactness, computational efficiency and the logarithmic mapping associated with the Lie group, allowing us to extend the PD-alike feedback control from pose-tracking to pose-following. As a result, the freedom and versatility of path-following is augmented to full body motions, i.e., translations, as well as rotations. To the best of our knowledge, this is the first work that explicitly attempts to follow upon both the longitudinal and angular coordinates.

[1]Autonomous Aerial Systems, School of Engineering and Design, Technical University of Munich, Germany. E-mail: jon.arrizabalaga@tum.de and markus.ryll@tum.de

[2]Munich Institute of Robotics and Machine Intelligence (MIRMI), Technical University of Munich

Notation: We will use $\dot{(\cdot)} = \frac{\mathrm{d}(\cdot)}{\mathrm{d}t}$ for time derivatives and $\mathring{(\cdot)} = \frac{\mathrm{d}(\cdot)}{\mathrm{d}\theta}$ for differentiating over pose-parameter θ. We denote three-dimensional vectors in bold $\boldsymbol{v}$, dual numbers as $a + \epsilon \mathrm{b}$ and dual quaternions as $\hat{q}$. We define $\hat{I}$ as $[1,0,0,0] + \epsilon[0,0,0,0]$. Operator $\circ$ is used for quaternion multiplications.

II. THE POSE-FOLLOWING PROBLEM

A. Rigid body dynamics

The three-dimensional rigid body dynamics in the body frame are described as

$$\ddot{\boldsymbol{p}}^b(t) = \boldsymbol{f}^b(t) m^{-1}\,, \tag{1a}$$

$$\dot{\boldsymbol{\omega}}^b(t) = \mathrm{J}^{-1}\left(\boldsymbol{\tau}^b(t) - \boldsymbol{\omega}^b(t) \times \mathrm{J}\,\boldsymbol{\omega}^b(t)\right)\,, \tag{1b}$$

where $\{\boldsymbol{p}^b, \boldsymbol{\omega}^b, \boldsymbol{f}^b, \boldsymbol{\tau}^b\} \in \mathbb{R}^3$ refer to the rigid body's position, angular velocity, control forces and control torques, while $m \in \mathbb{R}$ and $J \in \mathbb{R}^{3\times3}$ are the mass and inertia matrix. Given that frame superscripts remain constant, from now on they will be dropped. Taking position $\boldsymbol{p}$, longitudinal velocity $\dot{\boldsymbol{p}}$, attitude $q \in \mathrm{SO}(3)$ and angular velocity $\boldsymbol{\omega}$ as states $\boldsymbol{x}(t) = [\boldsymbol{p}(t), \dot{\boldsymbol{p}}(t), q(t), \boldsymbol{\omega}(t)]$ with forces $\boldsymbol{f}$ and torques $\boldsymbol{\tau}$ as inputs $\boldsymbol{u}(t) = [\boldsymbol{f}(t), \boldsymbol{\tau}(t)]$, and introducing the respective kinematic relationships, the dynamics in (1) can be written in the standard form:

$$\dot{\boldsymbol{x}}(t) = f(\boldsymbol{x}(t), \boldsymbol{u}(t))\,. \tag{2}$$

B. Geometric reference representation

Let Γ refer to a geometric reference set and be defined as a path with a moving frame attached to it. Its respective desired position and attitude are given by two functions, $\boldsymbol{p}_d : \mathbb{R} \to \mathbb{R}^3$ and $q_d : \mathbb{R} \to \mathrm{SO}(3)$, that depend on pose-parameter θ and are at least $\mathcal{C}^2$:

$$\Gamma = \{\theta \in [\theta_0, \theta_f] \subseteq \mathbb{R} \to \boldsymbol{p}_d(\theta) \in \mathbb{R}^3, q_d(\theta) \in \mathrm{SO}(3)\} \tag{3}$$

Notice that the C^2 requirement for q_d enables the calculation of the desired angular velocity $\boldsymbol{\omega}_d(\theta) : \mathbb{R} \to \mathbb{R}^3$ from its kinematic equations.

C. Problem statement

In order to incorporate the additional freedom inherited from path-following, we augment the rigid body dynamics in (2) by adding the pose-parameter $\theta(t)$ and its first time derivative $\dot{\theta}(t)$ as virtual states and assign the second time derivative $\ddot{\theta}(t)$ as a virtual input. Doing so results in

$$\dot{\boldsymbol{x}}_\Gamma(t) = f_\Gamma(\boldsymbol{x}_\Gamma(t), \boldsymbol{u}_\Gamma(t))\,, \tag{4}$$

where $\boldsymbol{x}_\Gamma(t) = \left[\boldsymbol{p}(t), \dot{\boldsymbol{p}}(t), q(t), \boldsymbol{\omega}(t), \theta(t), \dot{\theta}(t)\right]$ and $\boldsymbol{u}_\Gamma(t) = \left[\boldsymbol{f}(t), \boldsymbol{\tau}(t), \ddot{\theta}(t)\right]$. The augmented system f_Γ contains two additional equations of motion that relate to the integration chain of the pose-parameter $\theta(t)$, implying that the virtual input $\ddot{\theta}(t)$ is associated to its acceleration. Consequently, the time evolution $\theta(t)$, and thereby the pose reference $\{\boldsymbol{p}_d(\theta(t)), q_d(\theta(t))\}$, are controlled via the virtual input $\ddot{\theta}(t)$. This leads to the definition of the *pose-following error* as

$$\boldsymbol{e}_\Gamma(t) = \triangle\left[\{\boldsymbol{p}(t), q(t)\}, \{\boldsymbol{p}_d(\theta(t)), q_d(\theta(t))\}\right]\,, \tag{5}$$

where $\triangle : \left(\mathbb{R}^3, \mathrm{SO}(3)\right) \times \left(\mathbb{R}^3, \mathrm{SO}(3)\right) \to \mathbb{R}$ is a function that outputs the deviation between the rigid body's pose and reference pose, and will only be 0 if both are equal, i.e., $\triangle[a, b] = 0 \iff a = b$. Given the structure of $\mathrm{SE}(3)$, this function is dependent on the control design approach, and thus, will be defined in the upcoming Section III. For the remainder of this work, we address the following problem:

Problem 1 (**Pose-Following**)*: Given the geometric reference* Γ *in* (3) *and the augmented rigid body dynamics in* (4)*, formulate a controller* $\boldsymbol{u}_\Gamma(t) = \left[\boldsymbol{f}(t), \boldsymbol{\tau}(t), \ddot{\theta}(t)\right]$ *that fulfills:*

P1.1 ***Pose convergence:*** *The pose-following error vanishes asymptotically* $\lim_{t\to\infty} \boldsymbol{e}_\Gamma(t) = 0$.

P1.2 ***Convergence on pose-parameter:*** *The system converges to the end of the geometric reference* $\lim_{t\to\infty} \theta_f - \theta(t) = 0$.

Beyond that, for specific applications, it might be of interest to traverse the reference according to a desired velocity profile $\theta_{vd}(\theta(t))$:

Problem 2 (**Pose-Following with velocity assignment**)*: Given the geometric reference* Γ *in* (3) *and the augmented rigid body dynamics in* (4)*, formulate a controller* $\boldsymbol{u}_\Gamma(t) = \left[\boldsymbol{f}(t), \boldsymbol{\tau}(t), \ddot{\theta}(t)\right]$ *that fulfills:*

P2.1 *P1.1 from Problem 1*

P2.2 ***Velocity convergence:*** *The velocity of the pose-parameter converges to a desired velocity profile* $\lim_{t\to\infty} \dot{\theta}(t) - \theta_{vd}(\theta(t)) = 0$.

III. SOLUTION APPROACH

A. Mathematical preliminaries

To be concise, we skip the introductory mathematics linked with dual quaternions and adopt the notation and content presented in [22]. For more comprehensive details, we suggest consulting [21], [32], [33].

B. Unit dual quaternion error dynamics

The error between the pose of the rigid body (2) and the geometric reference (3) can be expressed in the form of a unit dual quaternion as

$$\hat{q}_e(t) = \hat{q}(t) \circ \hat{q}_d^*(\theta(t))\,, \tag{6}$$

and, after the derivations in Appendix B, the respective error dynamics can be expressed by the following model:

Model 1 (**Unit dual quaternion-based error dynamics**)*: For a given dual quaternion state* $\hat{q}(t)$ *and a desired configuration* $\hat{q}_d(\theta(t))$ *– associated to pose-parameter* $\theta(t)$ *–, the dynamics of the dual quaternion error in* (6) *are*

$$\dot{\hat{q}}_e(t) = \frac{1}{2}\hat{\omega}_e(t) \circ \hat{q}_e(t)\,, \tag{7a}$$

$$\hat{\omega}_e(t) = [0, \boldsymbol{\omega}_e(t)] + \epsilon\,[0, \dot{\boldsymbol{p}}_e(t) + \boldsymbol{p}_e(t) \times \boldsymbol{\omega}_e(t)]\,, \tag{7b}$$

$$\dot{\hat{\omega}}_e(t) = \hat{F}(t) + \hat{U}(t) + \ddot{\theta}(t)\, Ad_{\hat{q}_e(t)}\hat{\omega}_d^*(\theta(t)) + \tag{7c}$$

$$\dot{\theta}(t)\left[\dot{\hat{q}}_e(t) \circ \hat{\omega}_d^*(\theta(t)) \circ \hat{q}_e(t) + \hat{q}_e(t) \circ \dot{\theta}(t)\mathring{\hat{\omega}}_d^*(\theta(t)) \circ \hat{q}_e(t) + \hat{q}_e(t) \circ \hat{\omega}_d^*(\theta(t)) \circ \dot{\hat{q}}_e(t)\right]\,, \tag{7d}$$

where $Ad_{\hat{q}}\hat{V} = \hat{q} \circ \hat{V} \circ \hat{q}^*$, $\hat{q}_e(t) = \hat{q} \circ \hat{q}_d^*(\theta(t))$, $p_e(t) = p(t) + Ad_{q_e(t)}p_d^*(\theta(t))$, $w_e(t) = w(t) + \dot{\theta}(t)Ad_{q_e(t)}\omega_d^*(\theta(t))$, *and* $\hat{F}(t)$ *and* $\hat{U}(t)$ *are given in* (12d) *(see Appendix A).*

The initial two equations, namely the temporal derivative of the dual quaternion error and the dual twist error, exhibit a structure akin to that of pose-tracking. Nevertheless, distinctions emerge in the temporal derivative of the dual twist error, as it encompasses supplementary terms that are multiplied by the first and second time derivatives of the pose-parameter $\theta(t)$.

C. Control law

Given the error dynamics in (7), the *pose-convergence* definition in P1.1 can be reformulated as $\lim_{t\to\infty} \hat{q}_e(t) = \pm\hat{I}$ and $\lim_{t\to\infty} \hat{\omega}_e(t) = \hat{0}$. To achieve this, in this subsection we derive a control law for the term $\hat{U}$ in equation (7d). Its design is significantly influenced by the upcoming stability analysis. After determining the control law, we will be able calculate the command forces $\boldsymbol{f}$ and torques $\boldsymbol{\tau}$ from eq. (12d). In a similar way to [6] and [22], we decouple it into a feedforward (FF) and a feedback term (FB). The latter ensures stability, while the former eliminates nonlinearities in (7d):

$$\hat{U} = \hat{U}_{\text{FF}} + \hat{U}_{\text{FB}}\,. \tag{8}$$

It can be deduced from (7d) that the first and last term can be effortlessly eliminated by the feedforward compensation. However, this is not the case for the second adjoint term, which is multiplied by the virtual input $\ddot{\theta}(t)$. To address this, we opt for $\ddot{\theta}(t) = U_\theta(x_\Gamma(t))$, where $U_\theta(\cdot)$ denotes the yet-to-be-defined *pose-parameter control law* that relies on the augmented state vector $x_\Gamma(t)$ in (4). This selection permits us to integrate the adjoint term into the feedforward scheme[1]:

$$\begin{aligned}\hat{U}_{\text{FF}}(t, U_\theta) = &-\hat{F}(t) - U_\theta(x_\Gamma(t))\,\text{Ad}_{\hat{q}_e(t)}\hat{\omega}_d^*(\theta(t)) - \\ &\dot{\theta}(t)\Big[\dot{\hat{q}}_e(t) \circ \hat{\omega}_d^*(\theta(t)) \circ \hat{q}_e(t) + \\ &\hat{q}_e(t) \circ \dot{\theta}(t)\mathring{\hat{\omega}}_d^*(\theta(t)) \circ \hat{q}_e(t) + \hat{q}_e(t) \circ \hat{\omega}_d^*(\theta(t)) \circ \dot{\hat{q}}_e(t)\Big]\,.\end{aligned} \tag{9}$$

With regards to the feedback component, in accordance with the pose-tracking formulation outlined in [22], we employ the logarithmic mapping associated to the Lie group of unit dual quaternions to develop a proportional derivative feedback as

$$\hat{U}_{\text{FB}}(t) = -2\hat{\boldsymbol{k}}_p \odot \ln \lambda\hat{q}_e(t) - \hat{\boldsymbol{k}}_v \odot \hat{\omega}(t)\,, \tag{10}$$

where $\hat{\boldsymbol{k}}_p$ and $\hat{\boldsymbol{k}}_v$ are vector dual quaternion control gains and $\lambda \in \{-1, 1\}$ is a switching parameter to account for both equilibrium points $\pm\hat{I}$. This is defined as $\lambda = 1$, if $\hat{q}_{e_1}(t) >= 0$ and -1 otherwise, where $\hat{q}_{e_1}$ refers to the first component of $\hat{q}_e(t)$.

[1]Model 1 in (7) facilitates the conversion of $x_\Gamma(t)$ into a dual quaternion error and a dual twist error, as well as the conversion of these errors back into $x_\Gamma(t)$.

D. Stability analysis

In the current subsection, we establish the requisite conditions for control laws $\hat{U}$ and U_θ to almost global asymptotic stability.

Theorem 1 (**Stability of pose-following**). *Consider the geometric reference* (3)*, the augmented system* (4)*, the control law* $\hat{U}$ *in* (8) *with the feedforward and feedback terms in* (9) *and* (10)*, and suppose that the following conditions are satisfied:*

i *The dual quaternion control gains are chosen as* $\hat{\boldsymbol{k}}_p > \hat{0}$ *with* $k_{pd1} = k_{pd2} = k_{pd3}$*, i.e., equivalent terms in the dual part of* $\hat{\boldsymbol{k}}_p$*, and* $\hat{\boldsymbol{k}}_v > \hat{0}$.

ii *The pose-parameter control law ensures that the velocity of the pose-parameter is positive, i.e.,* $U_\theta(x_\Gamma(t)) \implies \dot{\theta}(t) > 0,\ \forall\,\theta \in [\theta_0, \theta_f]$.

Then, the closed-loop control scheme defined by system (2) *and control law* (8) *solves the pose-following Problem 1.*

Proof: Starting with *pose convergence* in P1.1, since the feedforward term (9) was designed to eliminate all the nonlinearities in (7d), substituting (8) in (7d) results in $\hat{\omega}_e = \hat{U}_{\text{FB}}$. In addition, considering that (16) also remains true for pose-following, the stability analysis in [22] holds. This implies that Model 2 converges to the closest equilibrium point $\{\pm\hat{I}, \hat{0}\}$ asymptotically, which directly translates to the fulfillment of pose convergence. Regarding *convergence on pose-parameter* in P1.2, combining the Lyapunov function $V = ||\theta(t) - \theta_f||^2$ with $\dot{\theta}(t) > 0$ – from (ii) – shows that θ_f is an asymptotically stable equilibrium point. □

Theorem 2 (**Stability of pose-following with velocity assignment**). *Consider the geometric reference* (3)*, the augmented system* (4)*, the control law* $\hat{U}$ *in* (8) *with the feedforward and feedback terms in* (9) *and* (10)*, and suppose that the following conditions are satisfied:*

i *The dual quaternion control gains are chosen as* $\hat{\boldsymbol{k}}_p > \hat{0}$ *with* $k_{pd1} = k_{pd2} = k_{pd3}$ *and* $\hat{\boldsymbol{k}}_v > \hat{0}$.

ii *The pose-parameter control law is given by* $U_\theta(x_\Gamma(t)) = -k_\theta\left(\dot{\theta}(t) - \theta_{vd}(\theta(t))\right) + \dot{\theta}(t)\mathring{\theta}_{vd}(\theta(t))$*, where* $k_\theta \in \mathbb{R}_{>0}$.

Then, the closed-loop control scheme defined by system (2) *and control law* (8) *solves the pose-following with velocity assignment Problem 2.*

Proof: The proof for *pose convergence* in P2.1 remains the same as P1.1 in Theorem 1. When it comes to *velocity convergence* in P2.2, the utilization of the Lyapunov function $V = ||\dot{\theta}(t) - \theta_{vd}(\theta(t))||^2$ in conjunction with $U_\theta(x_\Gamma(t))$ as given in (iii), and the recognition that $\ddot{\theta}(t) = U_\theta(x_\Gamma(t))$, indicates that the velocity of the pose-parameter asymptotically converges to the desired velocity profile. □

IV. EXPERIMENTS

To evaluate the efficacy of our approach, we examine two case studies. The first case-study centers on the fundamental characteristics of the developed control law, i.e., its almost global asymptotic stability and its ability to converge to a predetermined velocity profile. In the second case-study, we

showcase the benefits of the proposed pose-following control law over its precursor, the pose-tracking control law.

Numerical implementation: Throughout all assessments, the parameters remain constant at $m = 1\text{kg}$, $J = \text{diag}(0.01, 0.01, 0.01), \text{Kg/m}^{-2}$, $\hat{\boldsymbol{k}}_p = \hat{\boldsymbol{k}}_v = \hat{\mathbf{3}}$, and $k_\theta = 1$.

A. Almost global asymptotic stability on pose-following with velocity assignment

The primary objective of this study is to validate the findings of Theorem 2, which establishes the almost global asymptotic stability of pose-following with velocity assignment. When doing so, we aim to confirm that, irrespective of the initial state, the pose of the rigid body converges to the desired geometric reference. To this end, we initialize the system at four distinct poses and desire to demonstrate that this convergence is maintained regardless of the assigned velocity. In pursuit of this objective, we evaluate each initial condition using two distinct profiles, namely a slow profile with $\theta_{vd,\text{slow}} = 0.019$ and a fast profile with $\theta_{vd,\text{fast}} = 0.075$. As an exemplary geometric reference, we select the same three-dimensional curve as in [34], and to meet the specifications of (3), we assign a moving frame to it.

The motion profiles obtained by implementing the control law (8) – with the pose-parameter control $\hat{U}_\theta$ specified in Theorem 2 – to the rigid body dynamics in (2) are presented on the left-hand side of Fig. 1 in Appendix C. The motion profiles corresponding to the faster velocity profiles are shown using a solid line and their corresponding orientations, while those related to the slower profiles are depicted using dashed lines.

These motions exhibit two notable features. Firstly, they all display asymptotic convergence towards the geometric reference. Secondly, as expected, the motions related to the slower velocity profiles achieve convergence at an earlier stage compared to those related to the faster velocity profiles.

For a more through analysis, we focus on the purple case-study, which refers to the motion located at the top-left corner of Fig. 1(a.1) in Appendix C. A detailed view of this case is presented on the right-hand side of Fig. 1(b.2). It is hereby confirmed that the velocity of the pose-parameter, $\dot{\theta}(t)$, converges to the desired velocity profile, θ_{vd}. In order to achieve this, we have analyzed the convergence not only in slow (green) and fast (purple) *constant* velocity profiles but also in a *varying* sinusoidal profile (orange), as shown in Figure 1(b.3).

Finally, we demonstrate the significance of considering the presence of two equilibrium points, $\pm\hat{I}$, which are addressed in our approach using the switching term λ (10). In the same case-study mentioned in the previous paragraph, we exhibit that deactivating this switching term results in the control law converging only to $\hat{I}$, leading to an excessively long and large motion. This is evident from the position and quaternion errors, as well as from the resulting motions depicted in light gray in Fig.1(b.1-2).

B. Comparison to pose-tracking

After carefully analyzing the relevant properties of the presented control law, in this second case study, we compare the performance of the proposed pose-following approach against the pose-tracking method outlined in [22]. To achieve this objective, we have selected a planar sinusoidal curve with an attached moving frame as the geometric reference. The aim of this task is to traverse the geometric reference from a zero-velocity pose. However, during the navigation, a longitudinal and angular disturbance is introduced. To ensure a fair comparison, both the pose-tracking and pose-following methods have been fine-tuned to guarantee that the navigation time remains the same in the absence of any disturbances.

For this experiment, we have selected a desired velocity profile function that is dependent on the distance between the system and the geometric reference:

$$U_\theta(x_\Gamma(t)) = -k_\theta \left(\dot{\theta}(t) - \theta_{vd}(d_{e,\perp}(x_\Gamma(t)) \right) , \qquad (11)$$

where $d_{e,\perp}(x_\Gamma(t))$ represents the transverse distance to the geometric reference. Intuitively, when the system is far from the reference, it decelerates until it is near enough to increase its velocity. This function – $\theta_{vd}(d_{e,\perp}(x_\Gamma(t))$ – can be adjusted by the user to fit the system properties and the task at hand. We have designed three variations of this function: progressive (red), medium (orange), and conservative (blue). These velocity profiles, along with their corresponding motions, can be visualized in Figure 2 at the Appendix C.

Upon comparing it to the pose-tracking method (in magenta), we observe two key differences. Firstly, at the start of the trajectory, the tracking method exhibits a slight deviation from the reference due to the rigid body being stationary and needing to catch up with the moving time-reference. In contrast, the proposed pose-following method takes into account its initial state and gradually increases its velocity along the reference. Secondly, once the disturbance has ended, the augmented degree of freedom in the system enables all three variants to decelerate and converge back to the geometric reference. This phenomenon is evident in the evolution of $\dot{\theta}$. The convergence rate is directly related to the degree of conservativeness of the desired velocity profile mapping. Conversely, the pose-tracking method lacks this additional degree of freedom and has no choice but to catch up with the time-based reference, leading to a significant deviation error.

V. CONCLUSIONS

In this paper we have presented a pose-following control approach for rigid body dynamics based on unit dual quaternions. Initially, we have derived the equations of motion for the full pose error between the rigid body and the geometric reference in the form of a dual quaternion and dual twist. Subsequently, we have extended the original control law to account for nonlinearities arising from the introduction of auxiliary states associated with pose-following and designed the additional degree of freedom either to achieve convergence to a desired velocity profile or as a feedback mechanism. When doing so, we have also established almost global asymptotic stability. Lastly, we have validated our approach with two illustrative simulations.

REFERENCES

[1] O.-E. Fjellstad and T. I. Fossen, "Position and attitude tracking of auv's: a quaternion feedback approach," *IEEE Journal of Oceanic Engineering*, vol. 19, no. 4, pp. 512–518, 1994.

[2] D. T. Stansbery and J. R. Cloutier, "Position and attitude control of a spacecraft using the state-dependent riccati equation technique," in *Proceedings of the 2000 American Control Conference. ACC (IEEE Cat. No. 00CH36334)*, vol. 3. IEEE, 2000, pp. 1867–1871.

[3] T. P. Nascimento and M. Saska, "Position and attitude control of multi-rotor aerial vehicles: A survey," *Annual Reviews in Control*, vol. 48, pp. 129–146, 2019.

[4] J. Arrizabalaga, N. van Duijkeren, M. Ryll, and R. Lange, "A caster-wheel-aware mpc-based motion planner for mobile robotics," in *2021 20th International Conference on Advanced Robotics (ICAR)*. IEEE, 2021, pp. 613–618.

[5] J. Arrizabalaga and M. Ryll, "Towards time-optimal tunnel-following for quadrotors," in *2022 International Conference on Robotics and Automation (ICRA)*. IEEE, 2022, pp. 4044–4050.

[6] F. Bullo and R. M. Murray, "Proportional derivative (pd) control on the euclidean group," 1995.

[7] T. Lee, M. Leok, and N. H. McClamroch, "Geometric tracking control of a quadrotor uav on se (3)," in *49th IEEE conference on decision and control (CDC)*. IEEE, 2010, pp. 5420–5425.

[8] K. Sreenath, T. Lee, and V. Kumar, "Geometric control and differential flatness of a quadrotor uav with a cable-suspended load," in *52nd IEEE Conference on Decision and Control*. IEEE, 2013, pp. 2269–2274.

[9] F. A. Goodarzi, D. Lee, and T. Lee, "Geometric adaptive tracking control of a quadrotor unmanned aerial vehicle on se (3) for agile maneuvers," *Journal of Dynamic Systems, Measurement, and Control*, vol. 137, no. 9, p. 091007, 2015.

[10] B. Paden and R. Panja, "Globally asymptotically stable 'pd+'controller for robot manipulators," *International Journal of Control*, vol. 47, no. 6, pp. 1697–1712, 1988.

[11] L. Figueredo, B. V. Adorno, J. Y. Ishihara, and G. A. Borges, "Robust kinematic control of manipulator robots using dual quaternion representation," in *2013 IEEE International Conference on Robotics and Automation*. IEEE, 2013, pp. 1949–1955.

[12] G. Bledt, M. J. Powell, B. Katz, J. Di Carlo, P. M. Wensing, and S. Kim, "Mit cheetah 3: Design and control of a robust, dynamic quadruped robot," in *2018 IEEE/RSJ International Conference on Intelligent Robots and Systems (IROS)*. IEEE, 2018, pp. 2245–2252.

[13] D. Lee, A. K. Sanyal, E. A. Butcher, and D. J. Scheeres, "Finite-time control for spacecraft body-fixed hovering over an asteroid," *IEEE Transactions on Aerospace and Electronic Systems*, vol. 51, no. 1, pp. 506–520, 2015.

[14] N. Filipe and P. Tsiotras, "Adaptive position and attitude-tracking controller for satellite proximity operations using dual quaternions," *Journal of Guidance, Control, and Dynamics*, vol. 38, no. 4, pp. 566–577, 2015.

[15] Y. Wu, X. Hu, D. Hu, T. Li, and J. Lian, "Strapdown inertial navigation system algorithms based on dual quaternions," *IEEE transactions on aerospace and electronic systems*, vol. 41, no. 1, pp. 110–132, 2005.

[16] Y. Zu, U. Lee, and R. Dai, "Distributed motion estimation of space objects using dual quaternions," in *AIAA/AAS Astrodynamics Specialist Conference*, 2014, p. 4296.

[17] D. Gan, Q. Liao, S. Wei, J. Dai, and S. Qiao, "Dual quaternion-based inverse kinematics of the general spatial 7r mechanism," *Proceedings of the Institution of Mechanical Engineers, Part C: Journal of Mechanical Engineering Science*, vol. 222, no. 8, pp. 1593–1598, 2008.

[18] L. Kavan, S. Collins, C. O'Sullivan, and J. Zara, "Dual quaternions for rigid transformation blending," *Trinity College Dublin, Tech. Rep. TCD-CS-2006–46*, 2006.

[19] K. Daniilidis, "Hand-eye calibration using dual quaternions," *The International Journal of Robotics Research*, vol. 18, no. 3, pp. 286–298, 1999.

[20] D.-P. Han, Q. Wei, and Z.-X. Li, "Kinematic control of free rigid bodies using dual quaternions," *Int. J. Autom. Comput.*, vol. 5, no. 3, pp. 319–324, 2008.

[21] X. Wang, D. Han, C. Yu, and Z. Zheng, "The geometric structure of unit dual quaternion with application in kinematic control," *Journal of Mathematical Analysis and Applications*, vol. 389, no. 2, pp. 1352–1364, 2012.

[22] X. Wang and C. Yu, "Unit dual quaternion-based feedback linearization tracking problem for attitude and position dynamics," *Systems & Control Letters*, vol. 62, no. 3, pp. 225–233, 2013.

[23] N. Filipe and P. Tsiotras, "Rigid body motion tracking without linear and angular velocity feedback using dual quaternions," in *2013 European Control Conference (ECC)*. IEEE, 2013, pp. 329–334.

[24] F. Zhang and G. Duan, "Robust integrated translation and rotation finite-time maneuver of a rigid spacecraft based on dual quaternion," in *Aiaa guidance, navigation, and control conference*, 2011, p. 6396.

[25] X. Wang, C. Yu, and Z. Lin, "A dual quaternion solution to attitude and position control for rigid-body coordination," *IEEE Transactions on Robotics*, vol. 28, no. 5, pp. 1162–1170, 2012.

[26] M. M. Marinho, L. Figueredo, and B. V. Adorno, "A dual quaternion linear-quadratic optimal controller for trajectory tracking," in *2015 IEEE/RSJ International Conference on Intelligent Robots and Systems (IROS)*. IEEE, 2015, pp. 4047–4052.

[27] U. Lee and M. Mesbahi, "Constrained autonomous precision landing via dual quaternions and model predictive control," *Journal of Guidance, Control, and Dynamics*, vol. 40, no. 2, pp. 292–308, 2017.

[28] H. T. Kussaba, L. F. Figueredo, J. Y. Ishihara, and B. V. Adorno, "Hybrid kinematic control for rigid body pose stabilization using dual quaternions," *Journal of the Franklin Institute*, vol. 354, no. 7, pp. 2769–2787, 2017.

[29] F. F. Afonso Silva, J. José Quiroz-Omaña, and B. Vilhena Adorno, "Dynamics of mobile manipulators using dual quaternion algebra," *Journal of Mechanisms and Robotics*, vol. 14, no. 6, p. 061005, 2022.

[30] T. Faulwasser and R. Findeisen, "Nonlinear model predictive control for constrained output path following," *IEEE Transactions on Automatic Control*, vol. 61, no. 4, pp. 1026–1039, 2015.

[31] A. P. Aguiar, J. P. Hespanha, and P. V. Kokotovic, "Path-following for nonminimum phase systems removes performance limitations," *IEEE Transactions on Automatic Control*, vol. 50, no. 2, pp. 234–239, 2005.

[32] A. T. Yang, *Application of quaternion algebra and dual numbers to the analysis of spatial mechanisms*. Columbia University, 1963.

[33] B. Kenwright, "A beginners guide to dual-quaternions: what they are, how they work, and how to use them for 3d character hierarchies," 2012.

[34] S. Kumar and R. Gill, "Path following for quadrotors," in *2017 IEEE Conference on Control Technology and Applications (CCTA)*. IEEE, 2017, pp. 2075–2081.

APPENDICES

A. Unit dual quaternion dynamics

To transform the rigid body dynamics in (2) to a unit dual quaternions representation, we start by derivating the definition of dual quaternions, i.e., $\hat{q} = q + \epsilon/2\, p \circ q$, in time:

$$\dot{\hat{q}}(t) = \frac{1}{2}\hat{\omega}(t) \circ \hat{q}(t)\,, \tag{12a}$$

$$\hat{\omega}(t) = [0, \boldsymbol{\omega}(t)] + \epsilon\,[0, \dot{\boldsymbol{p}}(t) + \boldsymbol{p}(t) \times \boldsymbol{\omega}(t)] \tag{12b}$$

where $\hat{\omega}(t)$ is the dual twist. Taking its time derivative, we get

$$\dot{\hat{\omega}}(t) = \dot{\boldsymbol{\omega}}(t) + \epsilon\,(\ddot{\boldsymbol{p}}(t) + \dot{\boldsymbol{p}}(t) \times \boldsymbol{\omega}(t) + \boldsymbol{p}(t) \times \dot{\boldsymbol{\omega}}(t))\,, \tag{12c}$$

and combining it with the rigid body dynamics in (1), leads to

$$\begin{aligned}\dot{\hat{\omega}}(t) &= \left(\boldsymbol{a} + \mathrm{J}^{-1}\boldsymbol{\tau}\right) + \epsilon\left(\boldsymbol{f}/m + \dot{\boldsymbol{p}} \times \boldsymbol{\omega} + \boldsymbol{p} \times \left(\boldsymbol{a} + \mathrm{J}^{-1}\boldsymbol{\tau}\right)\right) \\ &= \underbrace{\boldsymbol{a} + \epsilon\,(\boldsymbol{p} \times \boldsymbol{a} + \dot{\boldsymbol{p}} \times \boldsymbol{\omega})}_{\hat{F}} + \underbrace{\mathrm{J}^{-1}\boldsymbol{\tau} + \epsilon\left(\boldsymbol{f}/m + \boldsymbol{p} \times \mathrm{J}^{-1}\boldsymbol{\tau}\right)}_{\hat{U}} \\ &= \hat{F}(t) + \hat{U}(t)\end{aligned} \tag{12d}$$

with $\boldsymbol{a} = \mathrm{J}^{-1}\boldsymbol{\omega} \times \mathrm{J}\,\boldsymbol{\omega}$. For readability, in the first two lines of (12d) dependencies on time $(\cdot)(t)$ have been omitted. Notice that $\hat{F}(t)$ is fully defined by the rigid body's state $\boldsymbol{x}(t)$, while the force and torque control inputs $\boldsymbol{u}(t)$ only appear in $\hat{U}(t)$.

B. Unit dual quaternion error dynamics

By applying the dual quaternion and twist definitions, it is possible to transform the geometric reference Γ in (3) into a desired dual quaternion and a desired dual twist:

$$\hat{q}_d(\theta) = q_d(\theta) + \epsilon/2\, p_d(\theta) \circ q_d(\theta)\,, \tag{13a}$$

$$\hat{\omega}_d(\theta) = [0, \boldsymbol{\omega}_d(\theta)] + \epsilon\,[0, \mathring{\boldsymbol{p}}_d(\theta) + \boldsymbol{p}_d(\theta) \times \boldsymbol{\omega}_d(\theta)]\,, \tag{13b}$$

where $\theta \in [\theta_0, \theta_f]$. Combining (13) with the kinematics in (12), the equations of motion for the desired pose are obtained:

$$\mathring{\hat{q}}_d(\theta) = \frac{1}{2}\hat{\omega}_d(\theta) \circ \hat{q}_d(\theta)\,, \tag{14a}$$

$$\begin{aligned}\mathring{\hat{\omega}}_d(\theta) = {} & [0, \mathring{\boldsymbol{\omega}}_d(\theta)] + \\ & \epsilon\,[0, \mathring{\ddot{\boldsymbol{p}}}_d(\theta) + \mathring{\boldsymbol{p}}_d(\theta) \times \boldsymbol{\omega}_d(\theta) + \boldsymbol{p}_d(\theta) \times \mathring{\boldsymbol{\omega}}_d(\theta)]\,,\end{aligned} \tag{14b}$$

From (14) it is apparent that in contrast to the pose-tracking case [22], the desired pose in (13) does not evolve according to *time* t, but with respect to the *pose-parameter* θ. Derivating the dual quaternion error (6) in time[2] leads to

$$\dot{\hat{q}}_e(t) = \dot{\hat{q}}(t) \circ \hat{q}_d^*(\theta(t)) + \dot{\theta}(t)\hat{q}(t) \circ \mathring{\hat{q}}_d^*(t)\,.$$

Combining it with (12a), (14a), (6) and the property $(\hat{q}_1 \circ \hat{q}_2)^* = \hat{q}_2^* \circ \hat{q}_1^*$ results in

$$\dot{\hat{q}}_e(t) = \frac{1}{2}\left(\hat{\omega}(t) \circ \hat{q}_e(t) + \dot{\theta}(t)\hat{q}_e(t) \circ \hat{\omega}_d^*(\theta(t))\right)\,.$$

[2]Time derivations over pose-parameter θ dependent variables, such as the $\hat{q}_d(\theta(t))$ requires using the chain rule, i.e., $\frac{\mathrm{d}(\cdot)}{\mathrm{d}t} = \frac{\mathrm{d}(\cdot)}{\mathrm{d}\theta}\frac{\mathrm{d}\theta}{\mathrm{d}t} = \mathring{(\cdot)}\dot{\theta}(t)$

Noticing that $\hat{q}_e \circ \hat{\omega}_d^* = (\hat{q}_e \circ \hat{\omega}_d^* \circ \hat{q}_e^*) \circ \hat{q}_e$, the equation above can be rearranged to

$$\dot{\hat{q}}_e(t) = \frac{1}{2}\left(\hat{\omega}(t) + \dot{\theta}(t)\hat{q}_e(t) \circ \hat{\omega}_d^*(\theta(t)) \circ \hat{q}_e^*(t)\right) \circ \hat{q}_e(t)\,,$$

which takes the same form as (12a):

$$\dot{\hat{q}}_e(t) = \frac{1}{2}\hat{\omega}_e(t) \circ \hat{q}_e(t)\,, \tag{15a}$$

$$\hat{\omega}_e(t) = \hat{\omega}(t) + \dot{\theta}(t)\mathrm{Ad}_{\hat{q}_e(t)}\hat{\omega}_d^*(\theta(t))\,. \tag{15b}$$

When compared to the pose-tracking case, the first time derivative of the pose-parameter $\dot{\theta}(t)$ appears to be multiplying the second term of the dual twist error. Similar derivations result in $p_e(t) = p(t) + \mathrm{Ad}_{q_e(t)}p_d^*(\theta(t))$ and $w_e(t) = w(t) + \dot{\theta}(t)\mathrm{Ad}_{q_e(t)}\omega_d^*(\theta(t))$. These expressions allow to ensure that the right-hand side of (15b) is equivalent to

$$\hat{\omega}_e(t) = [0, \boldsymbol{\omega}_e(t)] + \epsilon\,[0, \dot{\boldsymbol{p}}_e(t) + \boldsymbol{p}_e(t) \times \boldsymbol{\omega}_e(t)]\,. \tag{16}$$

For brevity, these derivations are omitted. In case of interest, the procedure follows the same steps as the ones outlined in Appendix B of [22]. Other than that, to fully define the error dynamics, we still need to compute the time derivative of the dual twist error. Towards this end, we take the time derivative of (15b), which results in (7d).

C. Results

See the figures in the next page.

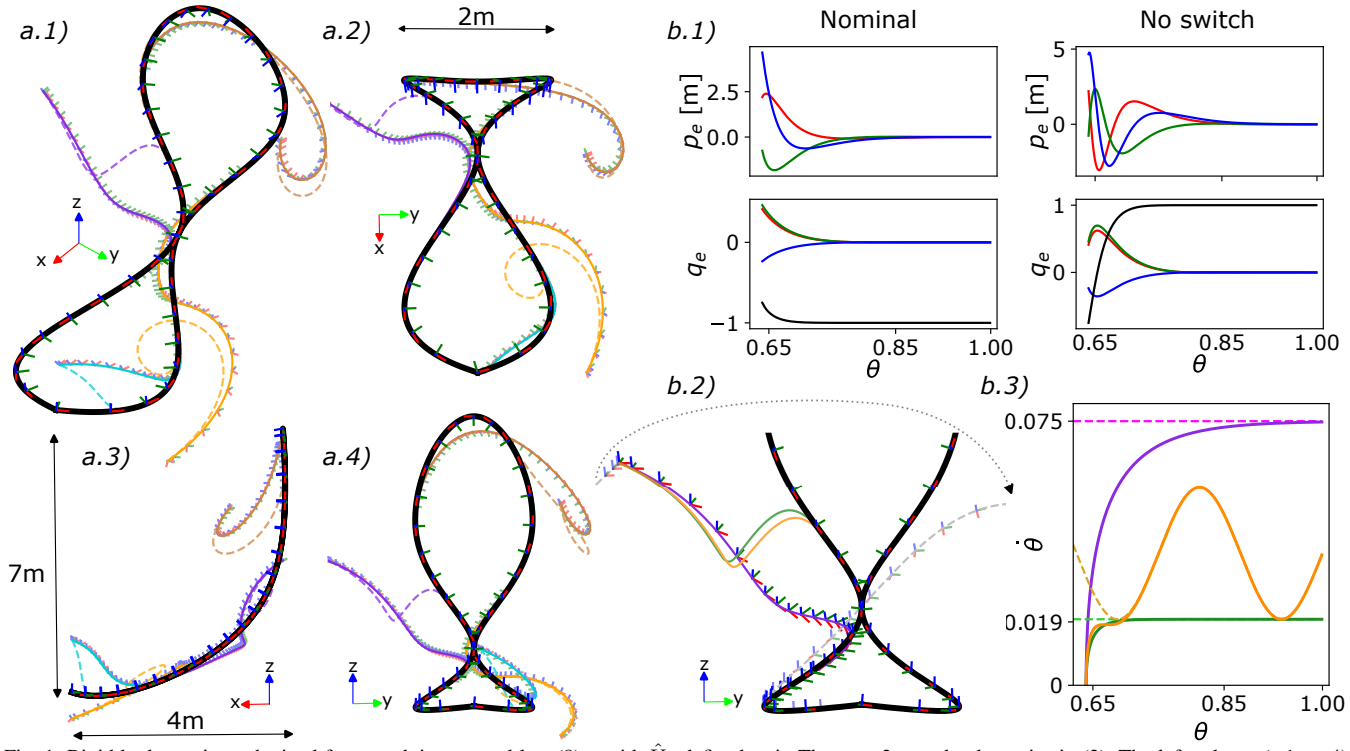

Fig. 1: Rigid body motions obtained from applying control law (8) – with $\hat{U}_\theta$ defined as in Theorem 2 – to the dynamics in (2). The left column (a.1 - a.4) shows the almost global asymptotic stability of the presented pose-following control law by starting from different initial poses (purple, orange, yellow, cyan) from different perspectives. Each starting point is evaluated according to two different constant velocity profiles. The motions associated to the fast profiles are depicted by a continuous line, as well as their orientations, while the motions related to the slow profiles are given by dashed lines. The plots at the top right (b.1), together with the gray dashed line in (b.2), showcase the consequences of deactivating the λ switch. The figure (b.3) shows that the pose-parameter's velocity (continuous line) converges to the desired velocity profile (dashed line) by evaluating three different cases (fast in purple, slow in green and sinusoidal in orange).

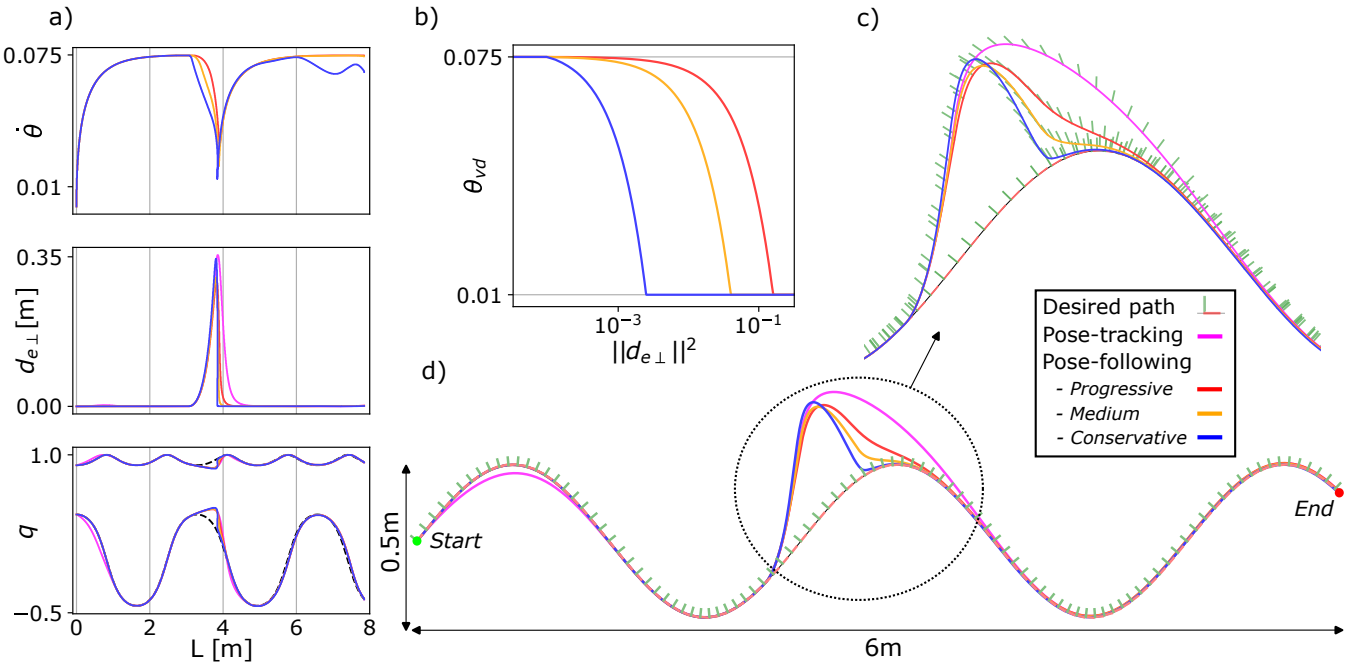

Fig. 2: A comparison between pose-tracking [22] (magenta) and three variants of the presented pose-following control approach (progressive as red, medium as orange and conservative as blue) in the presence of a disturbance. The geometric reference is given by a thin black line and its moving frame. For the rest of the motions, only the normal components are shown for clarity. a) From top to bottom, velocity of pose-parameter, transverse distance to the geometric reference and first and last components of the unit quaternion, where the dashed black line refers to the geometric reference's orientation. b) The desired velocity profile as a mapping from transverse distance to the reference. c) Zoomed comparison in the location of the disturbance and d) Overview of the case-study.